

A model of the bifurcated current sheet:

2. Flapping motions

M. I. Sitnov, M. Swisdak, J. F. Drake, and P. N. Guzdar

Institute for Research in Electronics and Applied Physics, University of Maryland, College Park, Maryland, USA

B. N. Rogers

Department of Physics and Astronomy, Dartmouth College, Hanover, New Hampshire, USA

Received 12 January 2004; revised 6 April 2004; accepted 9 April 2004; published 8 May 2004.

[1] A generalization of the *Harris* [1962] model has recently been proposed to explain the multi-spacecraft Cluster observations of thin bifurcated current sheets. It utilizes features of the ion motion in thin sheets and assumes anisotropy of the ion species. We report the results of 2D PIC simulations based on this model. Simulations confirm its self-consistency. They also reveal the lower-hybrid drift instability at the edges of the thinned sheet and a transition to a new quasi-equilibrium state with a considerable contribution of electrons to the bifurcated current. This can be explained using a modification of the original equilibrium model that assumes a small electron anisotropy. At later time instabilities of both parities are detected inside the sheet. They have much larger wavelengths and end up with the kink-type flapping motions of the bifurcated sheet as a whole.

INDEX TERMS: 2744 Magnetospheric Physics: Magnetotail; 7835 Space Plasma Physics: Magnetic reconnection; 7843 Space Plasma Physics: Numerical simulation studies.
Citation: Sitnov, M. I., M. Swisdak, J. F. Drake, P. N. Guzdar, and B. N. Rogers (2004), A model of the bifurcated current sheet: 2. Flapping motions, *Geophys. Res. Lett.*, 31, L09805, doi:10.1029/2004GL019473.

1. Introduction

[2] Finding bifurcated current sheets (BCSs) in the Earth's magnetotail and the detailed description of their 3D spatial structure and flapping motions [Nakamura *et al.*, 2002; Runov *et al.*, 2003; Sergeev *et al.*, 2003] has become by now one of the most significant accomplishments of the unique four-spacecraft Cluster mission. It has been found in particular that the current sheet (CS) can be very thin (a few thermal ion gyroradii based on the field outside) and yet split into two layers flapping in the north-south direction, with flapping waves propagating in both the dusk and dawn directions. Although BCSs have previously been detected in the tail [Sergeev *et al.*, 1993; Hoshino *et al.*, 1996], the new observations triggered a burst of modeling activity. The point is that the current bifurcation, which cannot be obtained from the standard CS model [Harris, 1962], might be explained nevertheless by a number of mechanisms. However, they do not conform to the new observations. For example, flapping itself gives rise to a bifurcation of the current occurrence frequency distribution [Karimabadi *et al.*, 2003], just as the probability of finding an oscillating

pendulum peaks off its minimum potential energy state. But, in the case of Cluster, the bifurcation has been detected in individual CS crossings [Sergeev *et al.*, 2003]. Another explanation might be reconnection effects related either to the Hall-MHD physics [Shay *et al.*, 1998] or to slow shocks [Hoshino *et al.*, 1996]. However, the new BCS observations revealed neither the dawn-dusk magnetic field component consistent with the Hall-MHD picture nor the plasma flows typical for slow shocks.

[3] The BCS effect may also arise because of the plasma anisotropy as was first demonstrated by Cowley [1978] for relatively thick sheets in the gyrotropic approximation. To introduce the effects of anisotropy in thin CSs Sitnov *et al.* [2003] extended the set of invariants of motion, which are used in the Harris model to form the distribution function, namely the total particle energy $W_\alpha = m_\alpha v^2/2 + q_\alpha \phi$ (ϕ is the electrostatic potential; $\alpha = e, i$) and the dusk component of the canonical momentum $P_{y\alpha} = m_\alpha v_y + (q_\alpha/c)A_y$ (we use here the GSM coordinate system), by including the so-called sheet invariant $I_z^{(\alpha)} = (1/2\pi) \oint m_\alpha v_z dz$. The latter invariant is an analog of the conventional magnetic moment for very thin CSs where the particle orbits may strongly differ from the Larmor circle. The model by Sitnov *et al.* [2003] (hereafter SGS model) has been shown to conform very well to the new BCS observations.

[4] However, the BCS flapping motions cannot be explained by the equilibrium theory. Also, it remains unclear if the given SGS equilibrium will be stable or transform into another equilibrium. Note here that the generalization of the Harris model assuming plasma anisotropy can be done with the original set of the invariants W_α and $P_{y\alpha}$ if one assumes a more general than linear combination of these invariants in the distribution function [Schindler and Birn, 2002; Mottez, 2003]. To address these issues we performed a set of 2D particle simulations starting from the SGS model and further explored the model itself. The results of these studies are reported below.

2. Equilibrium Model

[5] The SGS model is based on the set of electron and ion distributions

$$f_{0\alpha} \propto \exp\left(-\frac{2W_\alpha - \omega_{0\alpha} I_z^{(\alpha)}}{2T_{\parallel\alpha}} + \frac{v_{D\alpha} P_{y\alpha}}{T_{\parallel\alpha}} - \frac{\omega_{0\alpha} I_z^{(\alpha)}}{2T_{\perp\alpha}}\right) \quad (1)$$

where $T_{\parallel\alpha}$, $T_{\perp\alpha}$, $\omega_{0\alpha} = eB_0/m_\alpha c$ ($e = |q_\alpha|$), and $v_{D\alpha}$ are the parallel and perpendicular temperatures, the cyclotron

frequency, and constant drift speed parameter for the species α , respectively, and B_0 is the magnetic field outside the CS. The model input includes the temperature ratio $\tau = T_{\perp e}/T_{\perp i}$, the anisotropy parameters $\eta_\alpha = T_{\perp \alpha}/T_{\parallel \alpha}$, the mass ratio $\mu = m_e/m_i$, and the drift speed $w_{D\alpha} = v_{D\alpha}/v_{T\perp \alpha}$. The output consists of the effective plasma beta parameter $\beta_0 = 8\pi n_0 T_{\perp i}/B_0^2$ and the equilibrium profiles of the magnetic field $b = B_x/B_0$, electrostatic potential $\varphi = e\phi/T_{\perp i}$, plasma $n = n/n_0$ and current $j = J/j_0$ densities. Here $n_0 = \max(n)|_{\eta_\alpha=1}$, $j_0 = B_0/2\rho_{0i}$ and $\rho_{0\alpha} = v_{T\perp \alpha}/\omega_{0\alpha}$. We also normalize the electromagnetic potential $A_y = -aB_0\rho_{0i}$ (where $a = \int^\zeta b(\zeta')d\zeta'$ with $\zeta = z/\rho_{0i}$), coordinate $z = \rho_{0i}\zeta$, velocity $v_{y,z} = v_{\perp T\alpha}w_{y,z}$, and the invariant $I_z^{(\alpha)} = I^{(\alpha)}m_\alpha v_{T\perp \alpha}\rho_{0\alpha}$. The basic equations, which are written below assuming electron anisotropy and zero normal component of the magnetic field, include the Ampere's equation

$$b^2(a) = \frac{2\beta_0}{\pi} \sum_\alpha \frac{\delta_\alpha \tau_\alpha^{1/2}}{s_\alpha \mu_\alpha^{1/2}} \int_0^a da' \exp\left[-\frac{\eta_\alpha \varphi(a')}{s_\alpha \tau_\alpha}\right] \times \exp\left(-\frac{2\eta_\alpha w_{D\alpha} a'}{s_\alpha \tau_\alpha^{1/2} \mu_\alpha^{1/2}}\right) \int w_y dw_y dw_z F_\alpha(w_y, w_z, a'), \quad (2)$$

with $F_\alpha = \exp(-\eta_\alpha(w_y - w_{D\alpha})^2 - \eta_\alpha w_z^2 + (\eta_\alpha - 1)I^{(\alpha)})$, $s_i = 1$, $s_e = -1$, $\tau_i = 1$, $\tau_e = \tau$, $\mu_i = 1$, $\mu_e = \mu$, and $\delta_\alpha = \exp[-w_{D\alpha}^2 \eta_\alpha (\eta_\alpha - 1)]$, and the quasi-neutrality equation

$$2a\left(\eta_e w_{De} \tau^{-1/2} \mu^{-1/2} + \eta_i w_{Di}\right) + \varphi(\eta_e \tau^{-1} + \eta_i) = \sum_\alpha s_\alpha \left\{ \log \left[\int dw_y dw_z F_\alpha(w_y, w_z, a) \right] - w_{D\alpha}^2 \eta_\alpha (\eta_\alpha - 1) \right\}, \quad (3)$$

where

$$I^{(\alpha)}(a, w_y, w_z) = \frac{2}{\tau_\alpha^{1/2} \mu_\alpha^{1/2} \pi} \int_{a_0}^{a_1} \frac{da'}{b(a')} \times \sqrt{w_y^2 + w_z^2 + \frac{\varphi(a) - \varphi(a')}{s_\alpha \tau_\alpha} - \left[w_y + \frac{a' - a}{s_\alpha \tau_\alpha^{1/2} \mu_\alpha^{1/2}} \right]^2} \quad (4)$$

with $a_{0,1} = a - s_\alpha \tau_\alpha^{1/2} \mu_\alpha^{1/2} \{w_y \pm [w_y^2 + w_z^2 + s_\alpha^{-1} \tau_\alpha^{-1} (\varphi(a) - \varphi(a'))]^{1/2}\}$, and the additional restriction $a_0 = 0$ if the formal solution of the latter equation becomes negative. The general equations (2)–(3) are complemented by the condition $\eta_e w_{De} \tau^{-1/2} \mu^{-1/2} + \eta_i w_{Di} = 0$ to provide zero electrostatic field outside the CS. Figure 1 shows the solutions of these equations for the two cases used below to start simulations: $\tau = 1$, $\mu = 1/16$, $w_{Di} = 0.14$, $\eta_i = 1.2$, $\eta_e = 1$ (case 1), and $\tau = 1/4$, $\mu = 1/16$, $w_{Di} = 0.3$, $\eta_i = 2$, $\eta_e = 1$ (case 2), as well as for a modification of case 2 for anisotropic electrons with $\eta_e = 1.065$. The eigenvalues of the system of equations (2)–(4) obtained for cases 1 and 2 are given by $\beta_0 = 0.45$ and 0.605 , respectively.

3. Simulation Setup

[6] To explore the evolution of the SGS equilibria we perform 2D PIC simulations using the explicit code P3D [Zeiler *et al.*, 2002], which is parallelized using MPI routines with 3D domain decomposition and retains the full

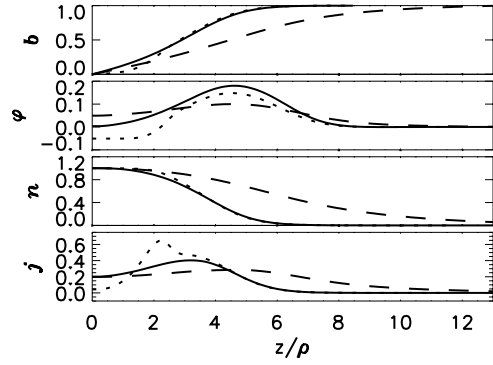


Figure 1. SGS model profiles b , φ , n (here normalized by $\max(n)$), and j for cases 1 (dashed lines), 2 (solid lines), and a modification of case 2 assuming electron anisotropy (dotted lines); $\rho = \rho_{0i}$.

dynamics for both ions and electrons. To load the complicated distribution of equation (1) we use the 3D rejection method [Press *et al.*, 1999] in the space (z, v_y, v_z) with the initial number of particles per grid $N_i = 600$ and the average number of accepted particles per grid $N_a = 21$ (case 1) and 12 (case 2). The CS was simulated in the boxes $(l_y/d, l_z/d) = (25.6, 25.6)$ (case 1) and $(51.2, 25.6)$ (case 2), where $d = c/\omega_{pi}$ is the ion inertial length based on the density n_0 , with the grids $N_y \times N_z = (1024, 1024)$ (case 1) and $(2048, 1024)$ (case 2). The speed of light is given by $c/v_A = 15$, where v_A is the Alfvén speed based on the maximum plasma density. The time step $\delta t = 0.005\omega_{0i}^{-1}$, with two substeps for fields, resolves both ω_{0e}^{-1} and ω_{pe}^{-1} , where ω_{pe} is the electron plasma frequency. The boundary conditions are periodic in the y -direction. In the z -direction the simulation box is bounded by conducting walls, where particles are specularly reflected.

4. Simulation Results

[7] In case 1 we detected no significant changes in the CS. Slight increases of the current and plasma densities (about 5% at the center) by the time $\omega_{0i}t = 10$ arise presumably because of the numerical limitations of the rejection procedure (finite size of the box along the direction v_y with $|v_y| \leq 3v_{T\perp i}$). No instabilities were detected up to $\omega_{0i}t = 30$ and the BCS structure shown in Figure 1 is preserved confirming the consistency of the SGS model. The BCS in this case with the halfwidth $L \sim 5-7\rho_{0i}$ is most consistent with the one observed during 1055–1107 UT on 29 August, 2001 [Runov *et al.*, 2003, 2004] with $B_0 = 20$ nT and $T_i \sim 4.3$ keV. Then $\rho_{0i} \approx 450$ km is just 4.5 times less than the half-distance between the bifurcated CSs, $\delta \sim 2000$ km.

[8] More interesting is case 2, when the BCS is approximately twice as thin as in case 1. First, as a result of the strong plasma density gradient at the outer edges of the split current, the lower-hybrid drift instability (LHDI) develops (Figures 2a–2c). As shown in Figure 3, the LHDI results in further enhancement of the current bifurcation due to the build-up of the bifurcated electron current. Moreover, the convergence of the current profiles suggests that the system approaches a new quasi-equilibrium state. The electron current bifurcation can be explained by the SGS model. According to Figure 1 (dotted lines), it may appear because

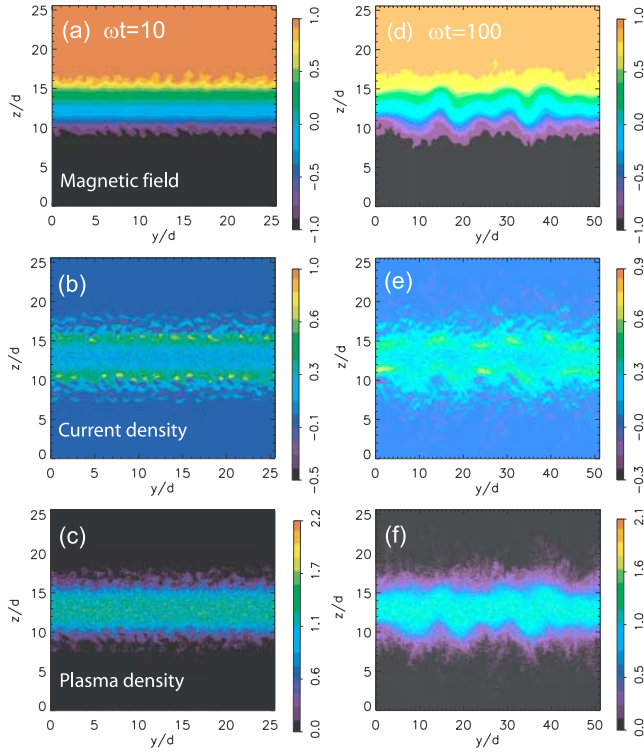


Figure 2. Color contours of the magnetic field B_x , current density j , and ion density n_i for $\omega t = 10$ (a–c) and 100 (d–f); $\omega = \omega_{0i}$, $d = c/\omega_{pi} = \beta_0^{-1/2}\rho_{0i} \approx 1.3\rho_{0i}$.

of a small electron temperature anisotropy. Note here that PIC simulations of the thin Harris CS reveal generation of the pancake anisotropy as a nonlinear effect of the LHDI [Ricci *et al.*, 2003]. In Figures 4a–4c the LHDI is shown in the form of the fast Fourier transform (FFT) analysis of the magnetic field B_x . In particular, Figure 4a reveals the broad spectrum of the excited waves with the maximum for the mode number $m = 32$, corresponding to the value of the parameter $k\rho_{0e}\tau^{-1/2} = 0.76 \sim 1$, characteristic of the LHDI [Huba *et al.*, 1980]. The mode structure across the sheet shown in Figure 4b suggests that the LHDI develops rather independently in each of the bifurcated CSs.

[9] A larger-scale instability develops after the saturation of the LHDI. According to Figure 4d, at $\omega_{0i}t = 30$ the spectrum is dominated by the mode $m = 3$, with the odd parity of the magnetic field B_x (Figure 4e). Having the same

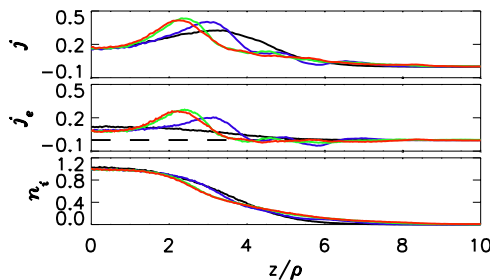


Figure 3. Changes in the total current j , electron current j_e and ion n_i densities averaged over the y -coordinate during the LHDI phase of the BCS evolution at $\omega_{0i}t = 0$ (black), 10 (blue), 20 (green) and 30 (red).

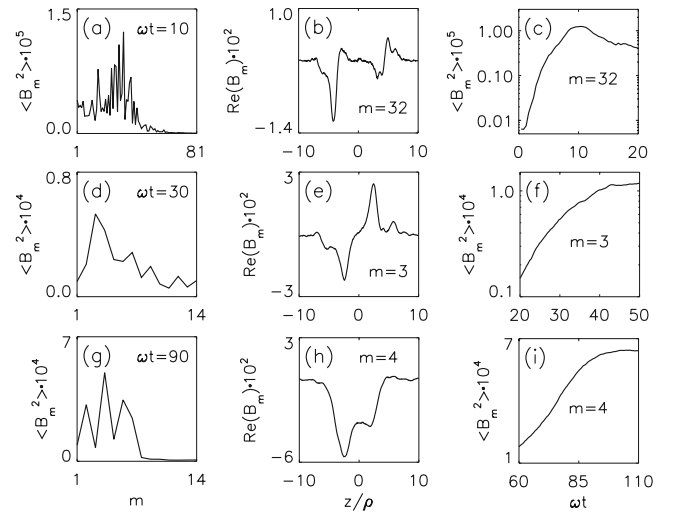


Figure 4. FFT analysis of the field B_x in case 2: (a, d, g) FFT spectra; (b, e, h) eigenmode profiles across the sheet for the modes with the given m from the left panel spectrum; (c, f, i) time history of the modes with the given m . B_m is the amplitude of the FFT transform with the mode number m ; $\langle B_m^2 \rangle$ is the corresponding intensity averaged over all z .

parity as the so-called sausage mode, which grows in the Harris CS for $\mu > 0.1$ [Silin *et al.*, 2002], this mode resembles rather the synchronized kink-type motions of two separate CSs. Note that the BCS flapping with the sausage parity was reported by Runov *et al.* [2003]. According to Figure 4f, this instability saturates at $\omega_{0i}t \sim 40$.

[10] Finally, the global kinking of the BCS develops (Figures 2d–2f; Figure 4h shows the mode parity). It is this type of flapping motions that was revealed in the analysis of the September 26, 2001 event [Sergeev *et al.*, 2003]. The wavelength of the kink mode with $m = 4$ (Figures 4g and 4h) is given by $\lambda \approx 16.5\rho_{0i}$, while its maximum amplitude $\delta z \approx 4\rho_{0i}$ approaches or even exceeds the equilibrium half-width of the BCS $L \approx 3-5\rho_{0i}$ (the lower and upper estimates of L are inferred from the profiles $b(z)$ and $j(z)$, respectively, shown in Figure 1). Assuming $\rho_{0i} = 600$ km this gives us the estimates $\lambda \approx 1.5R_E$ and $\delta z \approx 0.4R_E$ with $L \approx 1800-2400$ km, which are fairly consistent with observations [Runov *et al.*, 2003; Sergeev *et al.*, 2003]. According to Figure 4i, the growth rate of the BCS kink instability (hereafter BKI) $\gamma \sim 0.1\omega_{0i}$ is about two times less than that of the sausage-parity instability and an order of magnitude less than the LHDI growth rate. The value of γ is consistent with the growth rate of the drift-kink instability (DKI) [Daughton, 1999]. However, the BKI has also some features that distinguish it from the DKI and better fit the observations. In particular, the BKI phase speed $v_{BKI} \sim 0.1v_{\perp Ti}$ is three times less than that of DKI $v_{DKI} \sim v_{Di}$, while its frequency $\omega_{BKI} = 0.04\omega_{0i} \approx 0.1$ s $^{-1}$ is one and a half orders of magnitude less than the DKI frequency in this wavelength region $\omega_{DKI} \sim \omega_{0i} \approx 2.5$ s $^{-1}$ (with $k_y L \approx 3k_y \rho_{0i}$). The frequency of the flapping motions is $\omega_f \sim 0.035$ s $^{-1}$ [Sergeev *et al.*, 2003].

5. Discussion and Conclusion

[11] One of the main findings of the present study is the remarkable structural stability of the bifurcated current

sheets based on the SGS model. The initial bifurcation persists, notwithstanding the build-up of the electron current and various types of flapping motions. Due to plasma waves, the initial equilibrium based on the additional invariant I_z might transform into other types of equilibria with no dependence on I_z . However, the only transition to another type of equilibrium detected in simulations turns out to be still consistent with the original SGS model if one assumes a small (few percent) anisotropy of the electron species.

[12] The BCS stability observed in case 1 is consistent with Cluster observations, in which the flapping motions are detected not in the form of instabilities, but rather as CS eigenmodes propagating from the central sector of the magnetotail, where they are excited by an as yet unknown mechanism [Sergeev *et al.*, 2004]. Flapping motions in the form of instabilities appear in case 2 with the halved (as compared to case 1) BCS thickness. Note that although the ion anisotropy in case 2 is larger than the typical values found in the magnetotail with η_i up to 1.34 [Sitnov *et al.*, 2003, and references therein], it is fairly consistent with the properties of the ion species near the X-line [e.g., Shay *et al.*, 1998]. The small-scale instability picture in case 2 is consistent with the classical LHDI theory, while the large-scale BCS eigenmodes differ from those of the Harris CS. In particular, the kink modes with the proper amplitude and wavelength have relatively small frequency ($\omega \ll \omega_{0i}$) and phase speed ($v_{ph} \ll v_{Di}$). This difference may arise from different free energy sources of instabilities in the Harris CS and the BCS. Similar to the ion-ion kink instability [Karimabadi *et al.*, 2003], the BCS kink motions can be induced by the strong ion bulk-flow velocity shear (as seen from a comparison of two lower panels in Figure 1) rather than the relative drift of electrons and ions. Their stability properties are believed therefore to weakly depend on the mass ratio. Also, they are hardly affected by the preliminary growth and saturation of the LHDI, which is well separated in time from the BKI, according to Figures 4c and 4i.

[13] One cannot however exclude the possibility that the slow BKI wave is a combination (beat wave) of two DKI-type modes, one of which is fast and related to the fast duskward ion motion at the BCS edges, while the other mode is slow or even propagating in the dawn direction due to the corresponding ion flow at the BCS center (an example of the dawnward ion bulk flow is given in Figure 4 by Sitnov *et al.* [2003]). The latter interpretation is particularly interesting in view of observations by Sergeev *et al.* [2004] indicating both the dusk and dawn propagation of flapping motions in contrast to the classical DKI with only duskward propagation.

[14] The SGS model can become more unstable in 3D. For instance, the anisotropy can be reduced because of the mirror instability, although this is not evident in view of small values of β_0 characteristic of the BCS and strong deviations from gyrotopry provided by the non-guiding-

center ion motion. We plan to address these issues in our future studies.

[15] **Acknowledgments.** We thank F. V. Coroniti, P. L. Pritchett, A. V. Runov and V. A. Sergeev for interesting discussions. The work was supported by NASA grant NAG513047 and NSF/DOE grant ATM0317253 to the University of Maryland at College Park. The PIC simulations were performed at the National Energy Research Scientific Computing Center at the Lawrence Berkeley National Laboratory.

References

- Cowley, S. W. H. (1978), The effect of pressure anisotropy on the equilibrium structure of magnetic current sheets, *Planet. Space Sci.*, *26*, 1037.
- Daughton, W. (1999), The unstable eigenmodes of a neutral sheet, *Phys. Plasmas*, *6*, 1329.
- Harris, E. G. (1962), On a plasma sheath separating regions of oppositely directed magnetic fields, *Nuovo Cimento A-B*, *23*, 115.
- Hoshino, M., A. Nishida, T. Mukai *et al.* (1996), Structure of plasma sheet in magnetotail: Double-peaked electric current sheet, *J. Geophys. Res.*, *101*, 24,775.
- Huba, J. D., *et al.* (1980), Lower-hybrid-drift instability in field reversed plasmas, *Phys. Fluids*, *23*, 552.
- Karimabadi, H., P. L. Pritchett, W. Daughton *et al.* (2003), Ion-ion kink instability in the magnetotail: 2. Three-dimensional full particle and hybrid simulations and comparison with observations, *J. Geophys. Res.*, *108*(A11), 1401, doi:10.1029/2003JA010109.
- Mottez, F. (2003), Exact nonlinear analytic Vlasov-Maxwell tangential equilibria with arbitrary density and temperature profiles, *Phys. Plasmas*, *10*, 2501.
- Nakamura, R., W. Baumjohann, A. Runov *et al.* (2002), Fast flow during current sheet thinning, *Geophys. Res. Lett.*, *29*(23), 2140, doi:10.1029/2002GL016200.
- Press, W. H., *et al.* (1999), *Numerical Recipes in Fortran 77*, Cambridge Univ. Press, New York.
- Ricci, P., *et al.* (2003), 3D kinetic simulations of the onset of collisionless magnetic reconnection, *Eos Trans. AGU*, *84*(46), Fall Meet. Suppl., Abstract SH31A-1076.
- Runov, A., R. Nakamura, W. Baumjohann *et al.* (2003), Cluster observation of a bifurcated current sheet, *Geophys. Res. Lett.*, *30*(2), 1036, doi:10.1029/2002GL016136.
- Runov, A., *et al.* (2004), Properties of a bifurcated current sheet observed on August 29, 2001, *Ann. Geophys.*, in press.
- Schindler, K., and J. Birn (2002), Models of two-dimensional embedded thin current sheets from Vlasov theory, *J. Geophys. Res.*, *107*(A8), 1193, doi:10.1029/2001JA000304.
- Sergeev, V. A., D. G. Mitchell, C. T. Russell, and D. J. Williams (1993), Structure of the tail plasma/current sheet at 11 Re and its changes in the course of a substorm, *J. Geophys. Res.*, *98*, 17,345.
- Sergeev, V., *et al.* (2003), Current sheet flapping motion and structure observed by Cluster, *Geophys. Res. Lett.*, *30*(6), 1327, doi:10.1029/2002GL016500.
- Sergeev, V., *et al.* (2004), Orientation and propagation of current sheet oscillations, *Geophys. Res. Lett.*, *31*, L05807, doi:10.1029/2003GL019346.
- Shay, M. A., J. F. Drake, R. E. Denton, and D. Biskamp (1998), Structure of the dissipation region during collisionless magnetic reconnection, *J. Geophys. Res.*, *103*, 9165.
- Silin, I., *et al.* (2002), Instabilities of collisionless current sheets, *Phys. Plasmas*, *9*, 1104.
- Sitnov, M. I., P. N. Guzdar, and M. Swisdak (2003), A model of the bifurcated current sheet, *Geophys. Res. Lett.*, *30*(13), 1712, doi:10.1029/2003GL017218.
- Zeiler, A., D. Biskamp, J. F. Drake *et al.* (2002), Three-dimensional particle simulations of collisionless magnetic reconnection, *J. Geophys. Res.*, *107*(A9), 1230, doi:10.1029/2001JA000287.

J. F. Drake, P. N. Guzdar, M. I. Sitnov, and M. Swisdak, Institute for Research in Electronics and Applied Physics, University of Maryland, College Park, MD 20742, USA. (sitnov@astro.umd.edu)

B. N. Rogers, Department of Physics and Astronomy, Dartmouth College, Hanover, NH 03755, USA.